Radio Science, Volume 33, Number 4, Pages 1187–1197, July–August 1998

A ray tracing formulation and its application to some problems in over-the-horizon radar

C. J. Coleman

Wide Area Surveillance Division, Defence Science and Technology Organisation
Salisbury, South Australia, Australia

Abstract. A simple, two-dimensional ray tracing scheme is developed and is applied to several propagation problems of importance to over-the-horizon radar. In particular, it is used as the basis of schemes for the simulation of oblique and backscatter ionograms. The efficiency of the scheme makes it ideal for applications where fast calculations are required, and an algorithm for inverting backscatter ionogram leading edges is developed as a particular example.

1. Introduction

Over-the-horizon radar (OTHR) is made possible by the existence of complex propagation phenomena, which, in the case of sky wave radar, consist of ionospheric refraction. Besides the obvious need to model propagation for the purpose of OTHR performance predictions, there is a need for such modeling to assist in the real-time operation of these radars. In particular, propagation modeling is required to fulfill the coordinate registration (CR) requirement. CR is the process whereby radar coordinates (propagation time and beam azimuth) are transformed into geographic coordinates (longitude and latitude). There is no simple method for translating between these coordinates, and the necessary relationships can only be found by characterizing propagation over the radar coverage. Such a characterization is normally achieved by building an ionospheric map from the available ionosonde (vertical, oblique, and backscatter) observations and then ray tracing through this map. In order to satisfy the real-time requirements of the radar, the ray tracing and ionogram inversion must be extremely fast. Section 2 of this paper describes an efficient ray tracing scheme that can help fulfill much of this requirement.

Although OTHR functions such as frequency management can make direct use of the ionograms provided by ionospheric sounders, activities such as CR require their inversion. There exist well-developed techniques for the inversion of vertical ionograms [*Davies*, 1990], and these will not be considered any further in this paper. In the case of oblique and backscatter ionograms, however, the process of inversion is far less well developed. Obviously, an ability to simulate these ionograms is an important first step toward their inversion, and this will rely on a ray tracing algorithm of the sort described in the present paper. Oblique ionosondes measure the time of flight (normally expressed in terms of group range) and signal strength of radio waves propagating between two fixed points. Such measurements are performed for a range of frequencies and result in an oblique ionogram (a plot of signal strength as a function of time and frequency). Section 3 of this paper develops an algorithm for the simulation of oblique ionograms and demonstrates its effectiveness through simulations for which there existed observed ionograms and an independent ionospheric characterization. Backscatter ionosondes provide a means of investigating the ionosphere at locations that are inaccessible to vertical and oblique soundings [*Croft*, 1972]. They operate by propagating HF radio waves to remote locations from which a small amount of energy is returned by means of a backscatter mechanism. Measurements are made over a range of frequencies, and the returned power is plotted as a function of frequency and group range (a backscatter ionogram). Backscatter ionograms are an important element of OTHR frequency management [*Earl and Ward*, 1987]. They do, however, require skilled interpretation, and ionogram simulation is an important tool in unraveling the information they contain. *Dyson and Bennett* [1992] have developed simulation techniques for spherically symmetric ionospheres, and, more recently, *Coleman* [1997] and *Russell et al.* [1997] have developed techniques for studying more general ionospheres. Section 4 describes a backscatter simulation

Paper number 98RS01523.
0048-6604/98/98RS-01523$11.00

algorithm that is based on the ray tracing scheme of section 2 and gives some examples of its use in interpreting ionogram structure. The further step of inferring the underlying ionospheric structure is even more difficult, and a full inversion is virtually impossible due to poorly understood aspects such as sea backscatter and ionospheric radio wave absorption. Fortunately, the leading edge is an ionogram feature that is independent of such factors, and most investigators have concentrated on the information it contains. Various authors have considered leading edge inversions in terms of parameterized spherically stratified ionospheres [*Rao*, 1974; *Dyson*, 1991], and this has been extended to the situation where the parameters have a linear geographic dependence [*DuBruff et al.*, 1979]. For a spherically symmetric ionosphere, *Chuang and Yeh* [1977] have developed a method for deriving more general vertical structure. *Fridman and Fridman* [1994] use a combination of the leading edge profile and a vertical sounding to derive deviations from spherical symmetry in terms of a function of one variable (either the height or range from the sounder). This function was shown to satisfy an integral equation which Fridman and Fridman solved by means of the Tikhonov regularization method. As a further application of the ray tracing algorithm, section 5 develops an alternative leading edge inversion technique. In a fashion similar to the method of Fridman and Fridman, the approach seeks an ionospheric correction in terms of a function of range but is able to avoid the use of integral equations and their attendant problems. It does, however, require a considerable number of leading edge simulations as part of an iterative procedure, and so the efficiency of the current ray trace algorithm is crucial to the effectiveness of the approach. Section 5 concludes with some examples of the inversion of observed leading edges for the situation where there existed independent verification of the ionospheres.

2. The Ray Tracing Equations

For most HF radio waves, their propagation is sufficiently described by geometric ray theory and hence can be analyzed by means of ray tracing. Studies using a full three-dimensional ray tracing algorithm [*Coleman*, 1993] have shown that two-dimensional (2-D) ray tracing is acceptable for most ionospheric propagation, extreme situations such as propagation through ionospheric disturbances being the exception. In the 2-D case, propagation takes place in the plane of the great circle through the ray end points and will satisfy Fermat's principle of the form

$$\delta \int_T^R \mu(r, \theta)\left[\left(\frac{dr}{d\theta}\right)^2 + r^2\right]^{1/2} d\theta = 0 \tag{1}$$

with the variations over all paths that connect the start and end points (T and R). The variable r is the distance from the center of the Earth, and θ is an angular coordinate along the great circle. Neglecting magnetoionic effects, the refractive index μ can be expressed as

$$\mu = \left(1 - \frac{\beta N}{f^2}\right)^{1/2} \tag{2}$$

where N is the electron density (electrons per cubic centimeter) and $\beta = 8.05 \times 10^{-5}$. Denoting $dr/d\theta$ by r', the Lagrange equation for the above variational principle is

$$\frac{d}{d\theta}\left(\frac{\mu r'}{\sqrt{r'^2 + r^2}}\right) - \sqrt{r'^2 + r^2}\,\frac{\partial \mu}{\partial r} - \frac{r\mu}{\sqrt{r'^2 + r^2}} = 0 \tag{3}$$

and defining

$$Q = \mu r'(r'^2 + r^2)^{-1/2} \tag{4}$$

equation (3) may be reduced to a pair of first-order ordinary differential equations:

$$\frac{dQ}{d\theta} = \frac{r}{2\sqrt{\mu^2 - Q^2}}\frac{\partial \mu^2}{\partial r} + \sqrt{\mu^2 - Q^2} \tag{5}$$

$$\frac{dr}{d\theta} = \frac{rQ}{\sqrt{\mu^2 - Q^2}} \tag{6}$$

From these can be derived the equations

$$\frac{d(\delta Q)}{d\theta} = \frac{r}{\sqrt{\mu^2 - Q^2}}\left[\frac{\delta r}{2r}\left(\frac{\partial \mu^2}{\partial r} + \frac{\partial^2 \mu^2}{\partial r^2}\right) - \left(\frac{1}{2(\mu^2 - Q^2)}\frac{\partial \mu^2}{\partial r} - \frac{1}{r}\right)\left(\frac{\delta r}{2}\frac{\partial \mu^2}{\partial r} - Q\delta Q\right)\right] \tag{7}$$

$$\frac{d(\delta r)}{d\theta} = \frac{r}{\sqrt{\mu^2 - Q^2}} \cdot \left[\frac{\delta r Q}{r} + \delta Q - \frac{Q}{\mu^2 - Q^2}\left(\frac{\delta r}{2}\frac{\partial \mu^2}{\partial r} - Q\delta Q\right)\right] \tag{8}$$

that describe variations δr and δQ in the quantities r

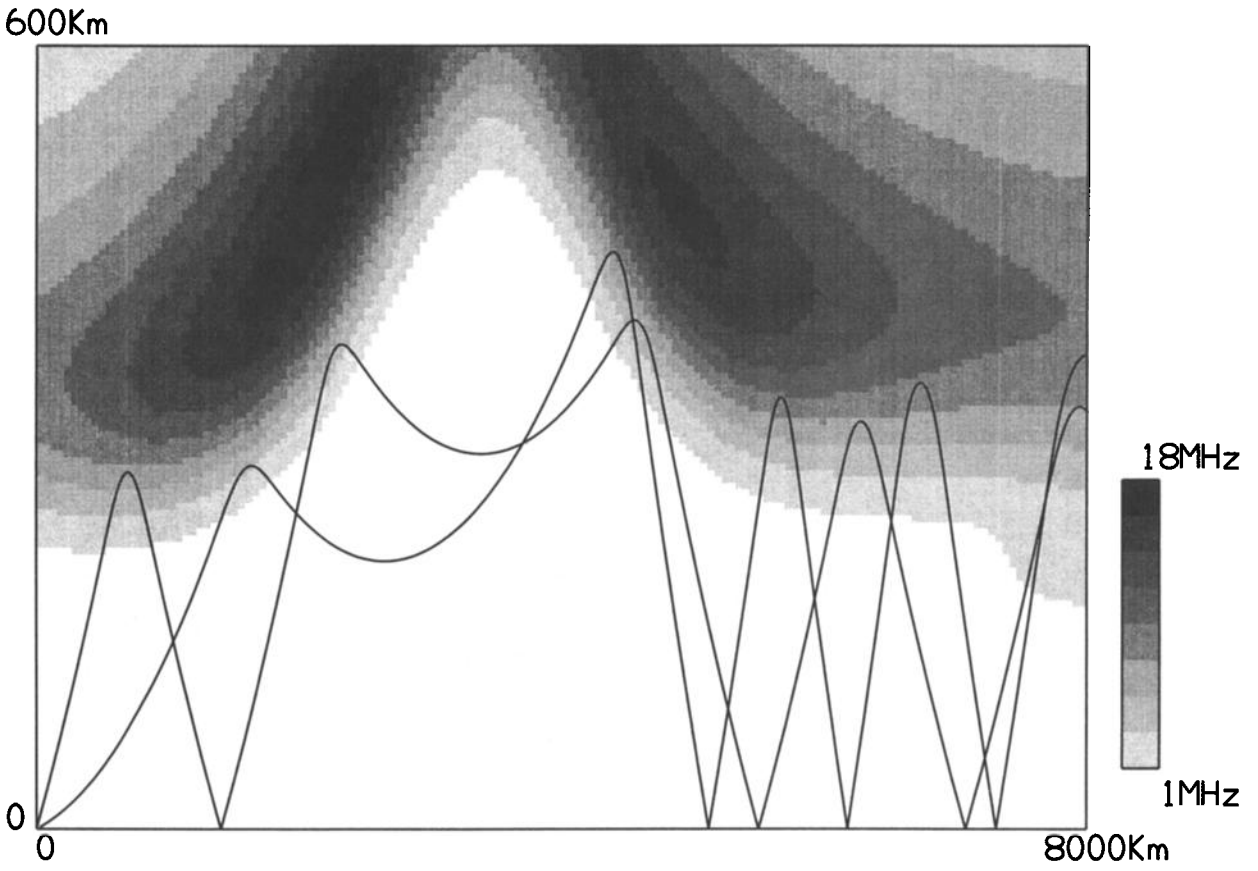

Figure 1. An example of ray tracing across the equatorial anomaly.

and Q. Such variations are useful for calculating the spreading of rays and hence the power of propagating radio waves.

Equations (5) and (6) can be rearranged into a more convenient form by use of the group path P' as an independent variable [*Coleman*, 1997]. Since $dP' = \mu^{-1}\, ds$, where $ds = (dr^2 + r^2 d\theta^2)^{1/2}$ is the distance element,

$$\frac{dP'}{d\theta} = \frac{\sqrt{r'^2 + r^2}}{\mu} \tag{9}$$

This, together with (5) and (6), yields the following system:

$$\frac{dQ}{dP'} = \frac{1}{2}\frac{\partial \mu^2}{\partial r} + \frac{\mu^2 - Q^2}{r} \tag{10}$$

$$\frac{dr}{dP'} = Q \tag{11}$$

$$\frac{d\theta}{dP'} = \frac{(\mu^2 - Q^2)^{1/2}}{r} \tag{12}$$

In the present work, equations (10)–(12) are solved by means of the Runge-Kutta-Fehlberg (RKF) adaptive numerical technique starting from initial values of r, θ, and Q (note that Q has the initial value sin ϕ for a ray that starts outside the ionosphere with takeoff angle ϕ). A major advantage of the current ray tracing equations is their avoidance of horizontal gradients, thus presenting a lighter computational load. When coupled with an efficient adaptive solver, they lead to a ray tracing scheme that is extremely fast and suitable for real-time applications.

Figure 1 shows the results of some rays traced northward from the Jindalee OTHR in central Australia on a frequency of 15 MHz (note that coordinate axes represent altitude and distance along the surface of the Earth). Propagation in this direction will

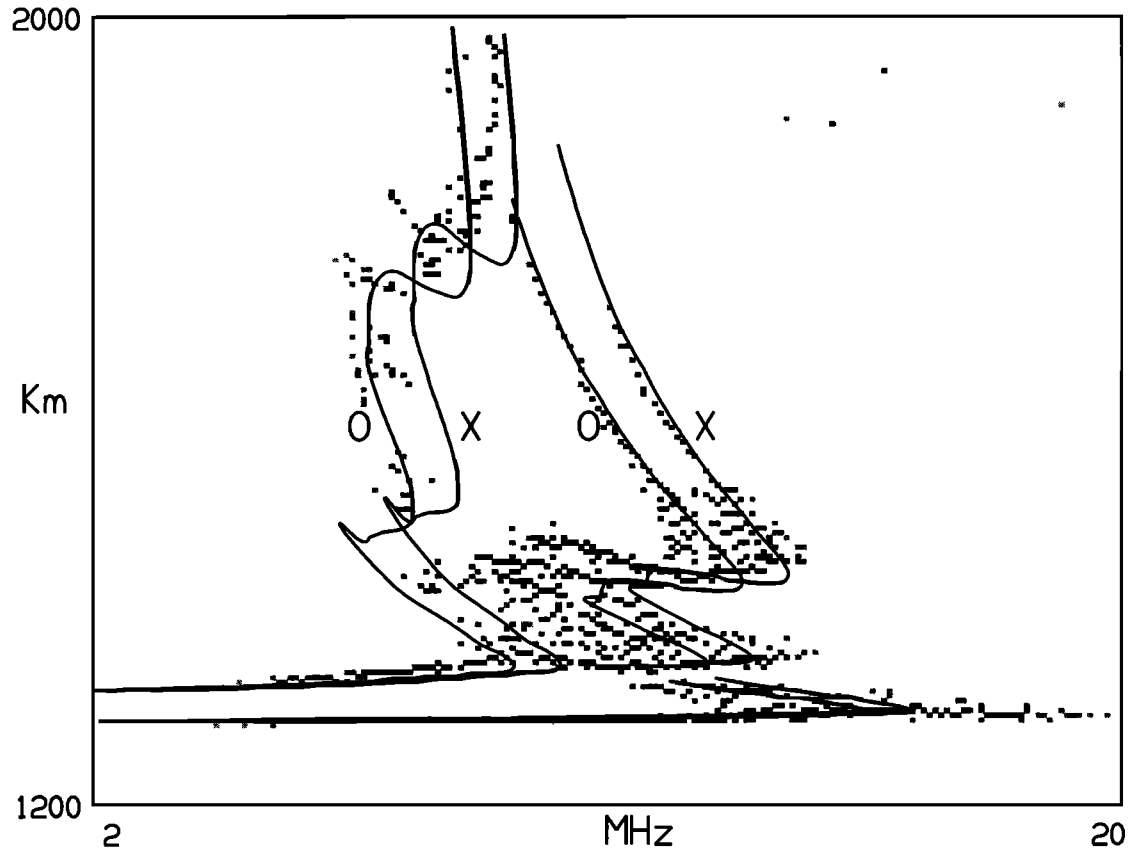

Figure 2. Simulation of an observed daytime oblique ionogram.

encounter the equatorial anomaly, and Figure 1 exhibits some of the chordal propagation that is characteristic of this direction. The figure superimposes ray paths over a plot of the corresponding plasma frequency (typical of a high sunspot equinox evening). The ionosphere was derived from a standard ionospheric model [*Coleman*, 1997] but is represented as a grid of electron density (sample intervals of 5 km in height and 100 km in range). For ray tracing purposes, all other values of the electron density N were calculated using the cubic interpolation

$$N = N_1 + \tfrac{1}{2}(N_2 - N_1)\left(\frac{h-h_1}{\Delta}\right) + (N_0 - \tfrac{5}{2}N_1 + 2N_2 - N_3) \cdot \left(\frac{h-h_1}{\Delta}\right)^2 + (\tfrac{1}{2}N_3 - \tfrac{3}{2}N_2 + \tfrac{3}{2}N_1 - \tfrac{1}{2}N_0)\left(\frac{h-h_1}{\Delta}\right)^3 \quad (13)$$

where h lies in the interval $[h_1, h_1 + \Delta]$, Δ is the mesh spacing, $N_0 = N(h_1 - \Delta)$, $N_1 = N(h_1)$, $N_2 = N(h_1 + \Delta)$, and $N_3 = N(h_1 + 2\Delta)$. This form of interpolation ensures that the approximation will be at least C^1 everywhere [*Coleman*, 1997]. Such an approach helps the efficiency of the algorithm and makes it easy to accommodate a large variety of ionospheres.

3. Oblique Ionogram Simulation

Oblique ionograms characterize HF ionospheric propagation between two fixed points and consist of a plot of received power in terms of group range and frequency. Their simulation needs point-to-point ray tracing and so requires an extension of the algorithm of section 2. Starting from one of the fixed points, a sparse fan of rays is launched in the direction of the other. If there exists a pair of consecutive rays that bracket the target point, a ray is traced at the mean elevation, and hence a pair of rays that better bracket the point is determined. The procedure is repeated until the desired end point has been located with sufficient accuracy. There can be several propagation

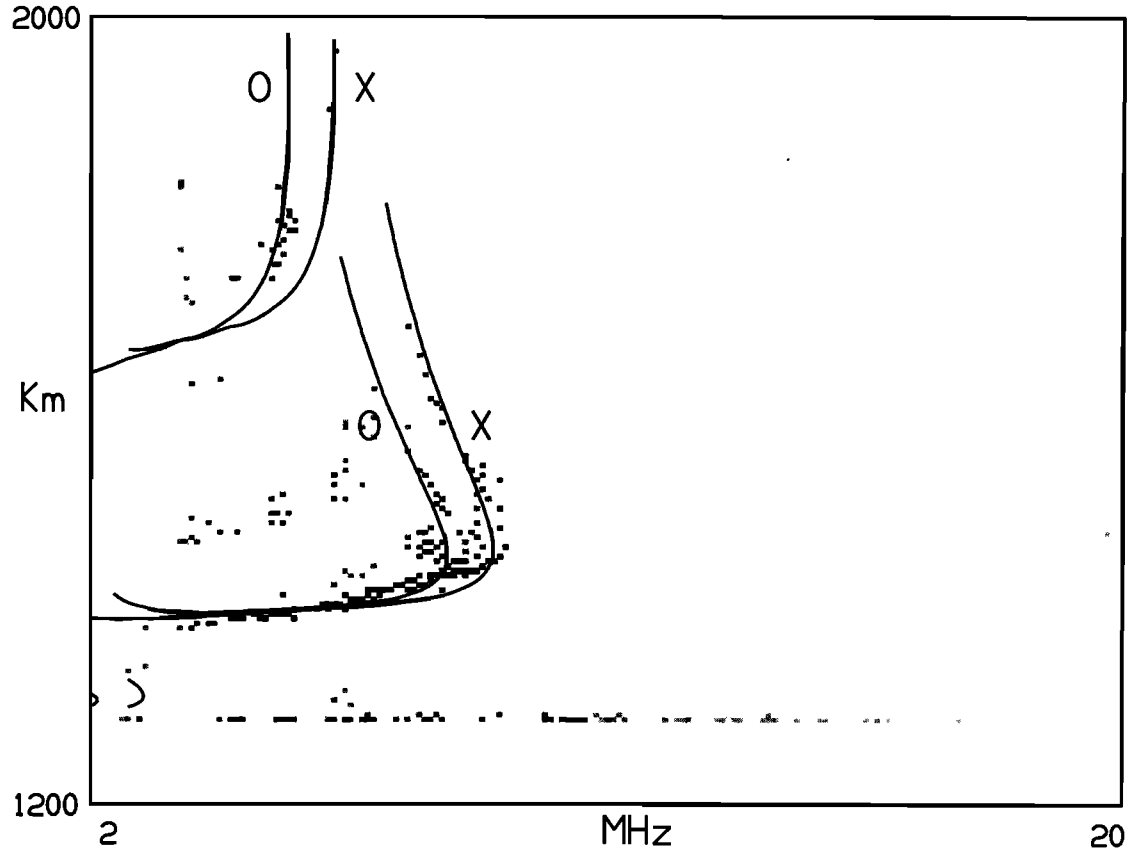

Figure 3. Simulation of an observed evening oblique ionogram.

modes (high and low rays, together with multihop) between the end points, and so the search of the sparse fan continues after the first propagation mode has been located. In order to produce an oblique ionogram, the above process is performed for a suitable range of frequencies.

Figures 2 and 3 show simulated ionograms for a path between Alice Springs and Darwin in Northern Territory, Australia. The simulated ionogram traces (solid lines for both O and X returns) are superimposed upon the corresponding observed ionograms (taken from an oblique ionosonde that operates as part of the Jindalee radar management system). For the simulation a spherically symmetric ionosphere was assumed, with vertical profile derived from an inversion of the corresponding vertical sounding at Elliot (a location almost midway between the transmitter and receiver). The inverted profile was converted into a vertical grid (5-km spacings) of electron density and other values calculated using the interpolation of section 2. Magnetoionic effects were estimated by use of an effective frequency approximation in which the field independent results are displaced in frequency by $\pm(1/2)f_H^L$, where f_H^L is the longitudinal gyrofrequency (midpath value). (This is an approximation that is based on a linearization of the refractive index in terms of the gyrofrequency and is very effective above 10 MHz.) It is possible to improve the approximation [*Bennett et al.*, 1994], but the above approach was found to be adequate for the current simulations. In addition, the group path needs to be corrected for magnetoionic effects, and a suitable correction term is given by $\pm(f_H^L/2f)(P' - P)$, where P is the phase path. (Once again, this approximation is readily derived by linearizing the refractive index in terms of gyrofrequency.) Other group path correction techniques have been developed [*Bennett et al.*, 1991], but the above approach is extremely simple and applies to a general ionosphere. Referring back to Figures 2 and 3, the correspondence between real and simulated ionograms is surprisingly good. It is clear, however, that sporadic E effects need to be

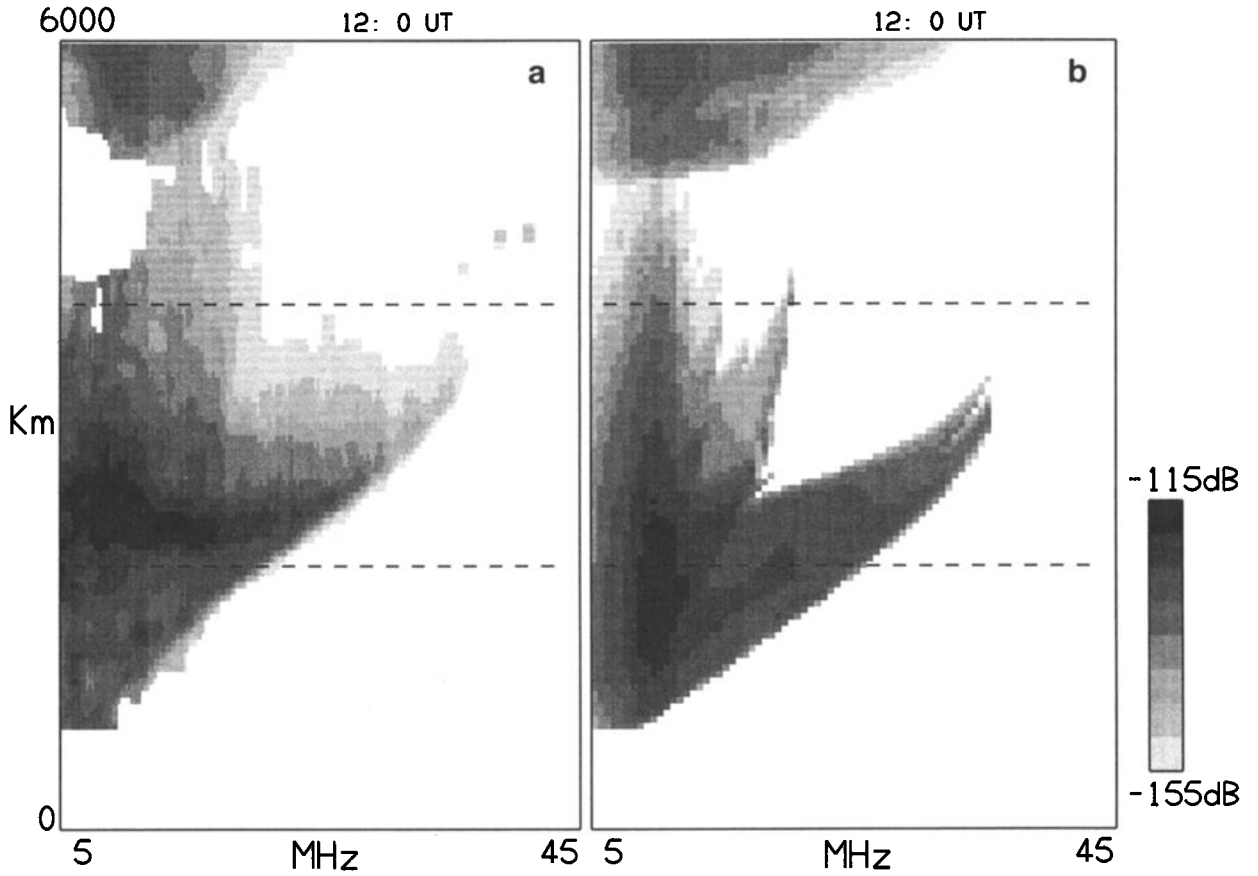

Figure 4. (a) Observed and (b) simulated backscatter ionograms.

included, and it is also likely that ionospheric gradients could be of importance.

4. Backscatter Ionogram Simulation

Backscatter ionograms characterize propagation to a large range of locations and consist of a plot of backscattered power in terms of frequency and group range. For a transmitter of power P_T, the radar equation gives the strength of backscatter from an area ΔA of the ground to be

$$P_R = \frac{\lambda^2 \sigma_0 \Delta A P_T}{(4\pi)^3 L d_T^2 d_R^2} G_T G_R \tag{14}$$

where d_T and d_R are effective distances along the outbound and return flux tubes. G_T and G_R are the transmit and receive antenna gains, respectively; λ is the wavelength; L is the attenuation due to ionospheric absorption; and σ_0 is the backscatter coefficient. In the present work, σ_0 is taken to be -23 dB (a value consistent with grazing incidence on a fully developed sea). The effective distance along a flux tube is calculated from the change in cross-sectional area of the tube and therefore includes the effects of focusing and defocusing. A backscatter ionogram is simulated by tracing ray fans for a range of frequencies, where each fan is produced by launching rays at a large number of sample elevations. For a set of representative ground ranges, each fan is searched for the possible combinations of outbound and return paths (nonreciprocal paths can be significant), and these two-way paths are used to calculate backscatter strength for a representative set of group ranges. The returned powers in a given group range cell are added incoherently to form the total power associated with this cell, and the process is repeated for all group range cells and frequencies. The ray tracing is achieved through the algorithm of section 2, and it is clear that its efficiency is crucial due to the large amount of ray tracing that is required.

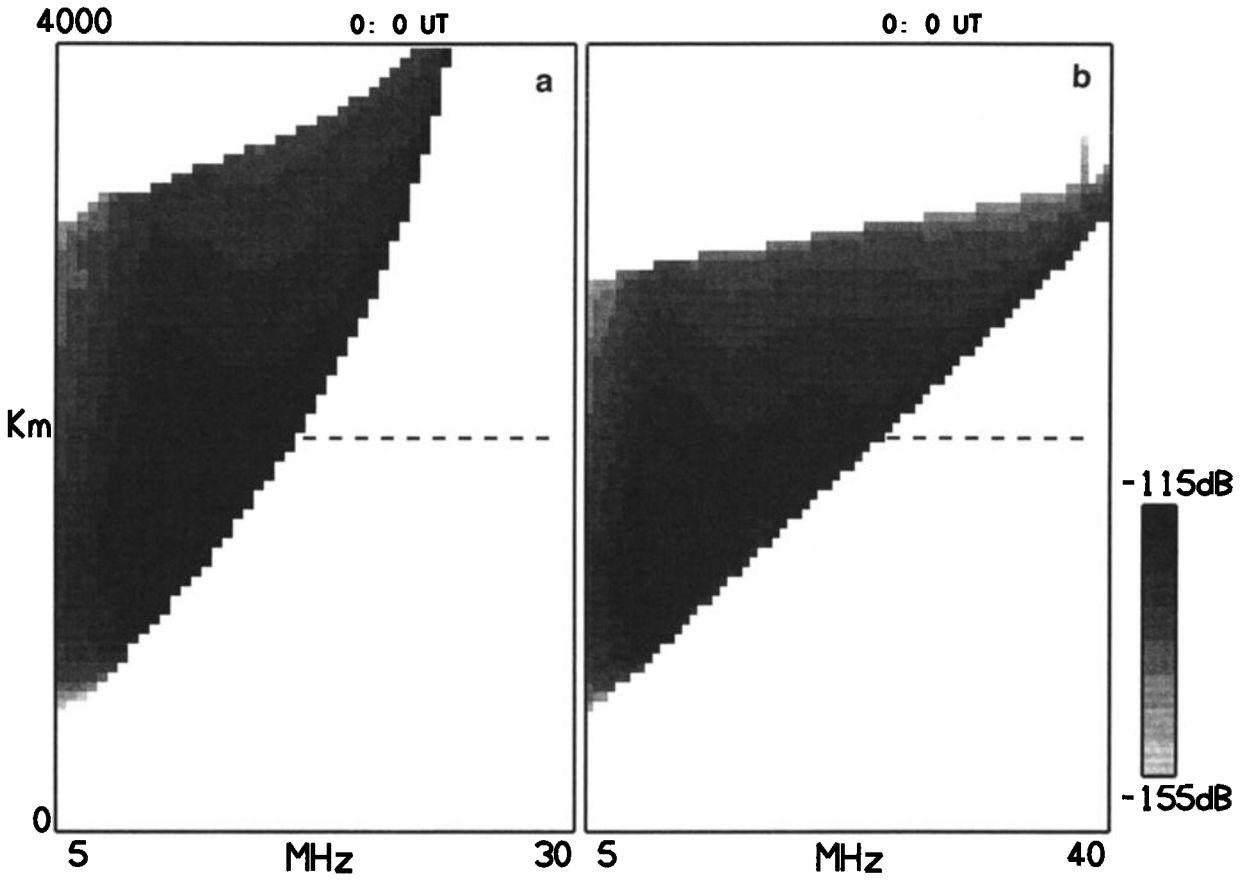

Figure 5. Some examples of leading edges from different ionospheres.

An example of a simulated backscatter ionogram is shown in Figure 4, together with the corresponding observed ionogram. The ionogram looks northward from Alice Springs, and its propagation must traverse the equatorial anomaly. It will be noted that the simulated ionogram shows much of the structure that occurs in the real case. In particular, both real and simulated ionograms show a reduction in returns from around the geomagnetic equator (a range of about 3500 km). Such ionogram features are not reproduced by virtual path ray tracing [*Davies*, 1990] and emphasizes the need for a more sophisticated approach at low latitudes. The ray tracing in Figure 1 was derived using the same ionosphere as the above example and clearly shows that the propagation hole is caused by the propagation skipping across the anomaly region by means of chordal modes.

Backscatter ionogram features can be markedly influenced by the structure of the underlying ionosphere, as can be seen from the above example. Most important among these features is the first-hop leading edge (the lower range limit across frequency when sporadic E is not present). Consider the leading edge simulations of Figure 5. Figure 5a was created using a spherically symmetric Chapman layer ionosphere and shows a leading edge with upward curvature that is characteristic of such symmetry. In Figure 5b the ionosphere has been modified by a linear gradient in the peak plasma frequency (the gradient was chosen to be of a similar order to that generated by the anomaly). It will be noted that the leading edge has straightened up in a manner that is often observed on ionograms looking northward from Alice Springs. Such effects have been pointed out by *Coleman* [1997] and *Russell et al.* [1997] and strongly support the notion that the leading edge carries useful information concerning horizontal ionospheric structure, a possibility that is exploited in the next section.

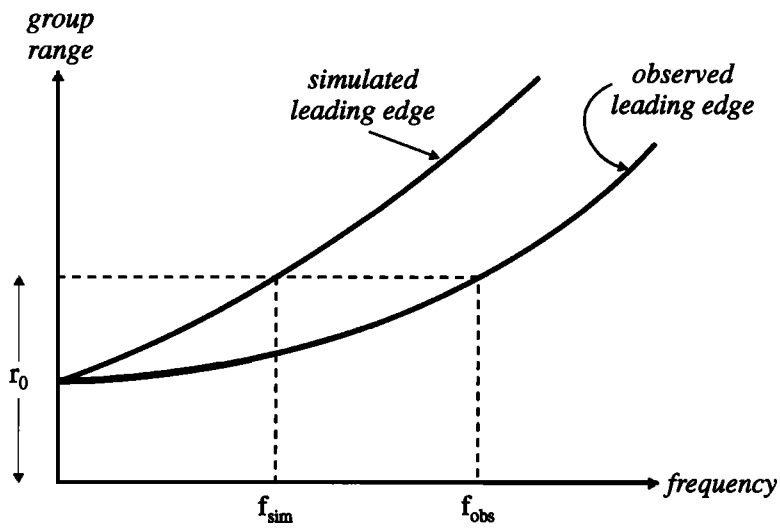

Figure 6. Leading edge parameters.

5. Backscatter Ionogram Inversion

Because of the large degree of uncertainty in many of the factors that influence backscatter strength, it would be difficult to implement a full backscatter ionogram inversion. For example, the sea backscatter coefficient can exhibit considerable geographic variations, and there is little prospect, at present, of gaining a reasonable characterization of this factor. Consequently, many authors have concentrated their efforts on ionogram features that are independent of backscatter strength, the foremost of these being the first-hop leading edge. There exist many techniques for inverting the leading edge [e.g., *Fridman and Fridman*, 1994], but the present paper develops an iterative approach that is based on simulations of the leading edge by means of numerical ray tracing. This requires a vast amount of ray tracing, and it is the efficiency of the current scheme that makes the approach viable. The basic idea behind the inversion is to simulate the leading edge for an ionosphere with suitable parameterization and to adjust the parameters until the simulated leading edge coincides with the observed edge. For a practical implementation this requires an ionosphere with a limited, and very carefully chosen, parameterization.

The leading edge is simulated by calculating the minimum group path on each of a representative set of sample frequencies. On each of these frequencies a fan of rays is traced over a selection of elevations and the minimum determined from this set. On the lowest frequency a fan is generated for an extensive range of elevation angles, but on subsequent frequencies, considerable efficiencies are achieved by only tracing those rays with elevations close to the minimum group path ray of the previous frequency. The technique for adjusting the ionosphere can be described as follows [*Coleman*, 1994]: First, note that the refractive index μ can be expressed as

$$\mu = \left(1 - \frac{f_p^2}{f^2}\hat{N}\right)^{1/2}$$

where $\hat{N}(r, \theta)$ is the electron density normalized on its peak value, with f_p the peak plasma frequency. From this, it will be noted that f_p and f always occur as a quotient, and so a given value of this quotient will result in the same ray however the value is achieved. Assume the electron density to be known up to a scaling factor (i.e., $\hat{N}$ is known, but f_p is not). If a wrong value of f_p is chosen, it can be compensated for by adjusting f. Similarly, a backscatter ionogram that is simulated using the wrong f_p can be corrected by adjusting the frequency scale. If the class of ionospheres (i.e., $\hat{N}$) is known, we merely need to simulate a backscatter ionogram for a typical f_p. Then, given an observed leading edge, the associated ionosphere (i.e., f_p) can be found by determining the frequency scaling that brings the observed and simulated leading edges together. The major problem is to find a suitable element from the class of candidate ionospheres. This could possibly be chosen from a histor-

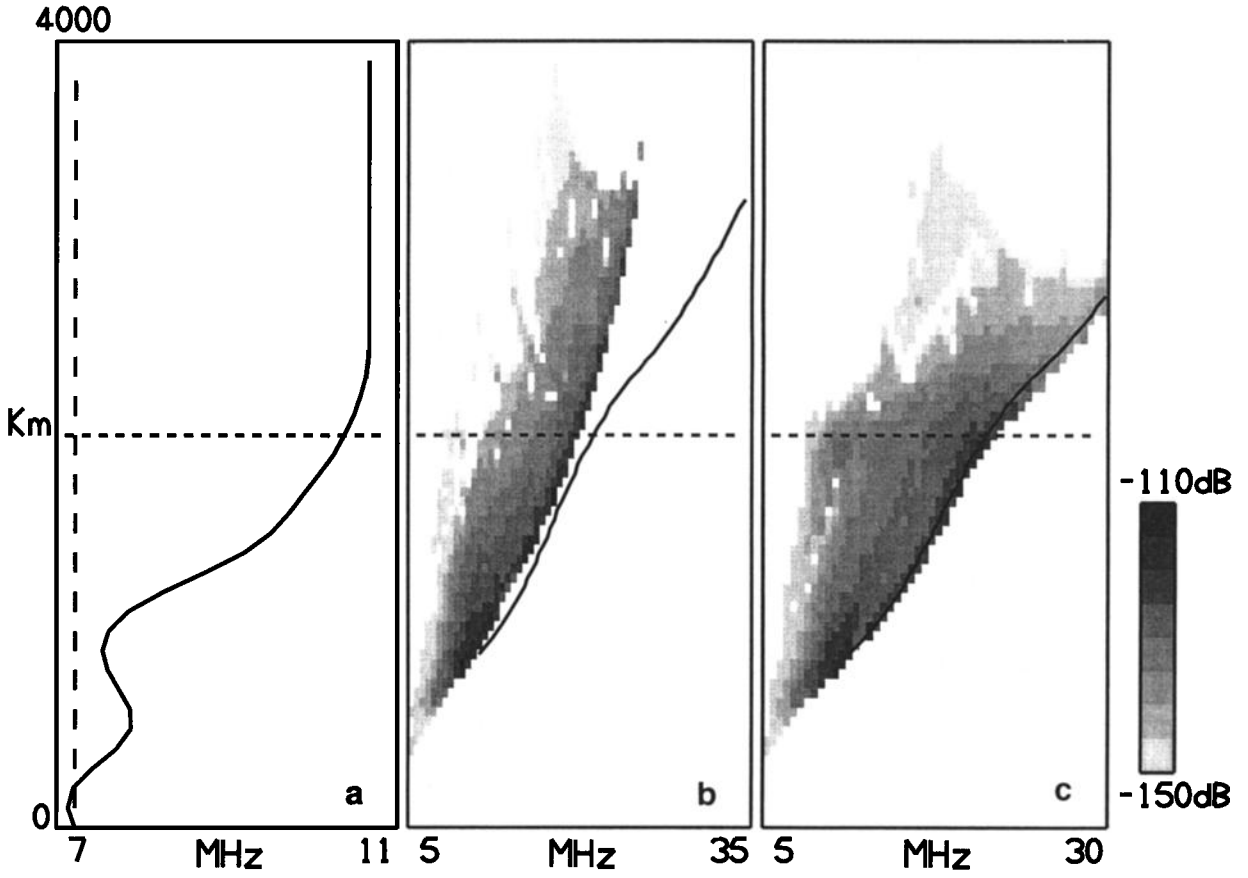

Figure 7. Inversion of a daytime leading edge: (a) initial (dashed line) and corrected (solid line) f_oF_2, (b) initial ionogram, and (c) corrected ionogram.

ical database of measured ionospheres or derived from a suitable model.

Although the above procedure is useful in its own right, it assumes that the structure of the ionosphere is already known up to a scaling factor. Since this is rarely the case, it is appropriate to ask whether the approach can be modified to yield more than a constant scaling factor. In particular, could such a modification provide information about horizontal structure. That the leading edge contains information concerning horizontal structure can be seen from the examples of simulated ionograms in section 3 (see Figure 5, for example).

Since the leading edge only provides a single dimension of data, it is insufficient for a full ionospheric inversion. *Fridman and Fridman* [1994] overcame this problem by limiting the structure either horizontally or vertically. In their second approach they assume an ionosphere for which the vertical profiles are similar at all locations (this class being determined by a supplementary vertical sounding) and use the leading edge to determine the scaling as a function of distance along the direction of propagation. In the present work a variant of this approach is used. An initial estimate of the ionosphere is determined and used to simulate a leading edge that is compared with the observed edge. For each range r_0, the frequency f_{obs} of the observed leading edge and the frequency f_{sim} of the simulated leading edge are determined (see Figure 6). Noting that the leading edge at a given frequency will be mainly influenced by the ionosphere around the geographic midpoint r_m between edge and sounder, the above considerations suggest that the plasma frequency at range r_m be modified by a factor that would bring the real and simulated leading edges together if applied everywhere. Consequently, the old plasma frequency f_p at the midpoint is replaced by $(f_{obs}/f_{sim})f_p$. This

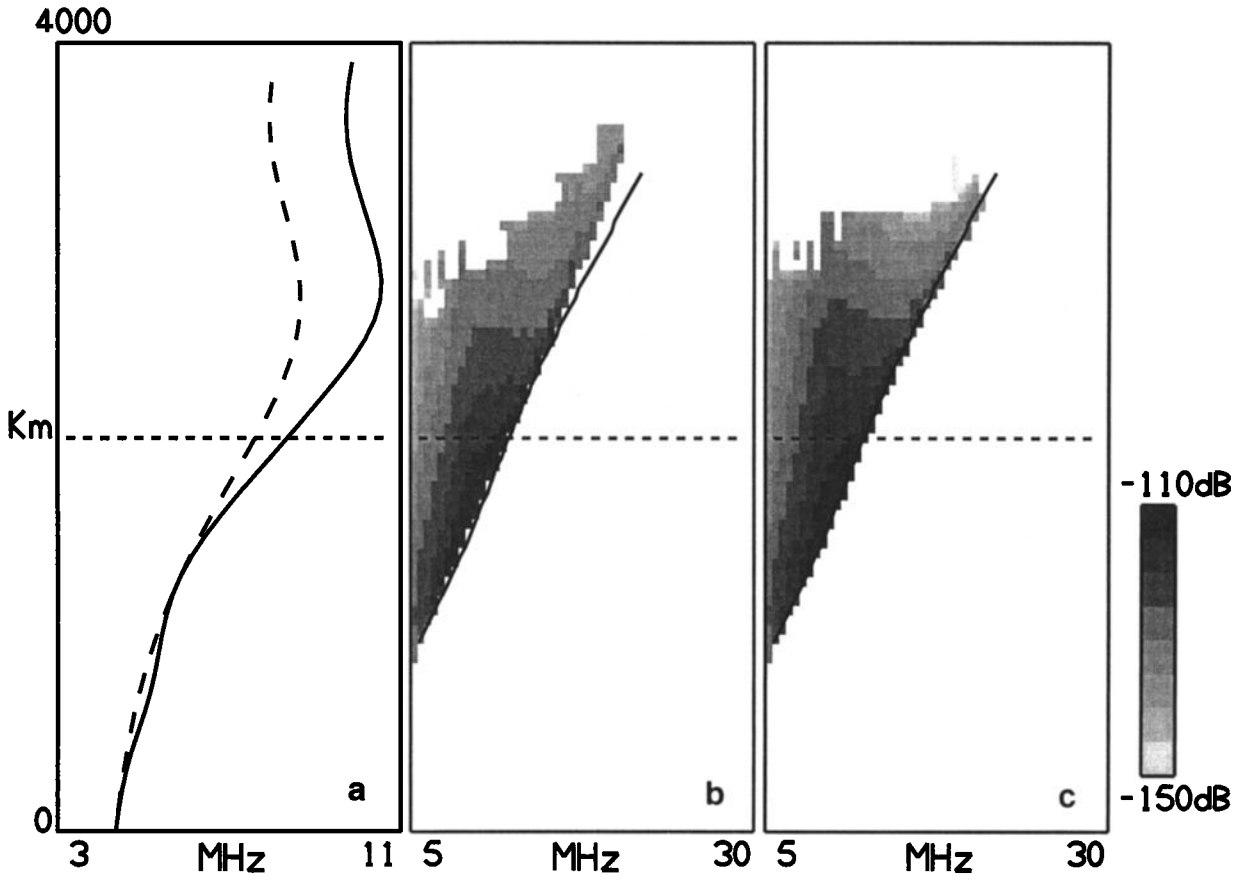

Figure 8. Inversion of an evening leading edge: (a) initial (dashed line) and corrected (solid line) f_oF_2, (b) initial ionogram, and (c) corrected ionogram.

process is repeated at all ranges r_0 for which both real and simulated edges exist. The shorter uncorrected ranges are then corrected with the factor for the shortest corrected range, and the longer are corrected with the factor from the longest corrected range. This process provides a new estimate for the ionosphere, and the whole procedure is repeated in an iterative fashion until the real and simulated leading edges are suitably close. During the development of the scheme it was found more effective to make the above adjustment at distances in excess of r_m (up to $1.4r_m$) for the highest ionogram frequencies. It was found that the early stages of iteration could experience some large variations in the position of the simulated ionogram tip and that the above procedure helped damp any harmful effects. There was, however, very little effect on the converged result.

The above algorithm is illustrated through its application to some real ionogram data that were collected during a recent campaign using the Jindalee OTHR. This radar has a system of vertical ionosondes as part of its prototype CR system, and it was possible to measure leading edges for a path that went through several of these. The sounders were located at Darwin (1280 km northward of the radar site), Alice Springs (the location of the radar), and Elliot (roughly halfway between the radar and Darwin). With this configuration it was possible to perform an operational test on the leading edge inversion algorithm. A spherically symmetric ionosphere with electron density profile derived from the Alice Springs vertical sounder was used as an initial estimate, and the leading edge algorithm was used to find a corrected ionosphere in the sounder direction. A particular example from late afternoon is shown in Figure 7. Figure 7a shows the variation of peak plasma frequency with range for the corrected ionosphere (the value for the uncorrected ionosphere is

superimposed), and the Figures 7b and 7c show the initial and corrected ionograms, respectively (the observed leading edge is superimposed). The measured values of peak plasma frequency at Elliot and Darwin were 7.6 and 9.3 MHz, and those predicted by the leading edge inversion were 7.8 and 9.5 MHz (the measured value at Alice Springs was 7.2 MHz). For this approach the daytime inversions were found to be very effective (when a good leading edge trace was available), but evening inversions were far less successful due to the large peak height gradients that occur at these times. After dusk, better results were obtained using initial ionospheres based on a global model that included peak height variations. Figure 8 shows the results for the inversion of a middle evening leading edge using an appropriate model initial estimate (it will be noted that the estimate of plasma frequency has a gradient appropriate to the anomaly). The measured values of peak plasma frequency at Elliot and Darwin were 4.8 and 5.6 MHz, and those predicted by the leading edge inversion were 5.1 and 5.8 MHz (the measured value at Alice Springs was 4.4 MHz). It will be noted that the major influence on the inversion is obtained from the longer ranges, and this has caused an increase in the anomaly strength.

6. Conclusion

The present paper has described a simple 2-D ray tracing algorithm and its application to some propagation problems of OTHR. In particular, the algorithm has been shown to be effective in simulating the output of some important ionosondes that support OTH radar operations. Such simulations can aid in the interpretation of the sensor output and thus increase their impact on radar operation. The ultimate goal is to invert the sensor output into ionospheric data, but this can be very difficult in the case of backscatter and oblique ionosondes. In the case of backscatter ionograms, however, it is possible to gain limited ionospheric information from the leading edge. It has been shown that the above ray tracing technique can form the basis of an effective algorithm for extracting such information, and this has been demonstrated by its application to leading edge data for which there existed independent verification of the underlying ionosphere.

References

Bennett, J. A., J. Chen, and P. L. Dyson, Analytic ray tracing for the study of HF magnetoionic radio propagation in the ionosphere, *Appl. Comput. Electromagn. Soc. J., 56*, 192–210, 1991.

Bennett, J. A., J. Chen, and P. L. Dyson, Analytic calculation of O- and X-mode nose frequencies on oblique ionograms, *J. Atmos. Sol. Terr. Phys., 56*, 631–636, 1994.

Chuang, S. L., and K. C. Yeh, A method for inverting oblique sounding data in the ionosphere, *Radio Sci., 12*, 135–140, 1977.

Coleman, C. J., A general purpose ionospheric ray tracing procedure, *Tech. Rep. SRL0131TR*, Def. Sci. and Technol. Organ., Salisbury, South Aust., Australia, 1993.

Coleman, C. J., A coordinate registration algorithm based on numerical ray tracing, *Res. Rep. RR-0009*, Def. Sci. and Technol. Organ., Salisbury, South Aust., Australia, 1994.

Coleman, C. J., On the simulation of backscatter ionograms, *J. Atmos. Sol. Terr. Phys., 59*, 2089–2099, 1997.

Croft, T. A., Sky-wave backscatter: A means for observing our environment at great distances, *Rev. Geophys., 10*, 73–155, 1972.

Davies, K., *Ionospheric Radio, IEE Electromagn. Waves Ser.*, vol. 31, Peter Peregrinus, London, 1990.

DuBroff, R. E., N. Narayana Rao, and K. C. Yeh, Backscatter inversion in spherically asymmetric ionosphere, *Radio Sci., 14*, 837–841, 1979.

Dyson, P. L., A simple method of backscatter ionogram analysis, *J. Atmos. Sol. Terr. Phys., 53*, 75–88, 1991.

Earl, G. F., and B. D. Ward, The frequency management system of the Jindalee over-the-horizon backscatter HF radar, *Radio Sci., 22*, 275–291, 1987.

Fridman, O. V., and S. V. Fridman, A method of determining horizontal structure of the ionosphere from backscatter ionograms, *J. Atmos. Sol. Terr. Phys., 56*, 115–131, 1994.

Rao, N., Inversion of sweep frequency sky wave backscatter leading edge for quasi-parabolic ionospheric layer parameters, *Radio Sci., 9*, 845–847, 1974.

Rusell, C. J., P. L. Dyson, Z. Houminer, J. A. Bennett, and L. Li, The effect of large-scale ionospheric gradients on backscatter ionograms, *Radio Sci., 32*, 1881–1897, 1997.

C. J. Coleman, Wide Area Surveillance Division, Defence Science and Technology Organisation, L200, P.O. Box 1500, Salisbury, South Australia 5108, Australia. (e-mail: chris.coleman@dsto.defence.gov.au)

(Received October 23, 1997; revised January 26, 1998; accepted February 9, 1998.)